Ott, L. (1977) in *An Introduction to Statistical Methods and Data Analysis*, pp 378-408, Duxbury Press, North Scituate, MA.
Patel, D. J., Kozlowski, S. A., Ikuta, S., & Itakura, K. (1984) *Biochemistry 23*, 3218-3226.
Patel, D. J., Shapiro, L., Kozlowski, S. A., Gaffney, B. L., & Jones, R. A. (1986a) *Biochemistry 25*, 1027-1036.
Patel, D. J., Shapiro, L., Kozlowski, S. A., Gaffney, B. L., & Jones, R. A. (1986b) *Biochemistry 25*, 1036-1042.
Pauly, G. T., Powers, M., Pei, G. K., & Moschel, R. C. (1988) *Chem. Res. Toxicol. 1*, 391-397.
Rhodes, D., & Klug, A. (1981) *Nature 292*, 373-380.
Rice, J., Crothers, D. M., Pinto, A. L., & Lippard, S. J. (1988) *Proc. Natl. Acad. Sci. U.S.A. 85*, 4158-4161.
Saenger, W. (1984) in *Principles of Nucleic Acid Structure*, pp 116-158, Springer-Verlag, New York.
Sancar, A., & Sancar, G. B. (1988) *Annu. Rev. Biochem. 57*, 29-67.
Singer, B., & Kusmierek, J. T. (1982) *Annu. Rev. Biochem. 52*, 655-693.
Sowers, L. C., Fazakerly, G. V., Kim, H., Dalton, L., & Goodman, M. F. (1986) *Biochemistry 25*, 3983-3988.
Toorchen, D., Lindamood, C., Swenberg, J. A., & Topal, M. D. (1984) *Carcinogenesis 5*, 1733-1735.
Topal, M. D., & Fresco, J. R. (1976) *Nature 263*, 289-293.
Ulanovsky, L., Bodner, M., Trifonov, E. N., & Choder, M. (1986) *Proc. Natl. Acad. Sci. U.S.A. 83*, 862-866.
Voigt, J. M., Van Houten, B., Sancar, A., & Topal, M. D. (1989) *J. Biol. Chem. 264*, 5172-5176.
Wang, J. C. (1979) *Proc. Natl. Acad. Sci. U.S.A 76*, 200-203.
Werntges, H., Steger, G., Riesner, D., & Fritz, H. (1986) *Nucleic Acids Res. 14*, 3773-3790.
Wu, H.-M., & Crothers, D. E. (1984) *Nature 308*, 509-513.
Zell, R., & Fritz, H. (1987) *EMBO J. 6*, 1809-1815.

Structural Studies of Bean Pod Mottle Virus, Capsid, and RNA in Crystal and Solution States by Laser Raman Spectroscopy†

Tiansheng Li,‡ Zhongguo Chen,§ John E. Johnson,§ and George J. Thomas, Jr.*,‡
Division of Cell Biology and Biophysics, School of Basic Life Sciences, University of Missouri—Kansas City, Kansas City, Missouri 64110-2499, and Department of Biological Sciences, Purdue University, West Lafayette, Indiana 47907
Received October 3, 1989; Revised Manuscript Received January 18, 1990

ABSTRACT: Structures of protein and RNA components of bean pod mottle virus (BPMV) have been investigated by use of laser Raman spectroscopy. Raman spectra were collected from both aqueous solutions and single crystals of BPMV capsids (top component) and virions (middle and bottom components, which package, respectively, small and large RNA molecules). Analysis of the data permits the assignment of conformation-sensitive Raman bands to viral protein and RNA constituents and observation of structural similarities and differences between solution and crystalline states of BPMV components. The Raman results show that the protein subunits of the empty capsid contain between 45% and 55% β-strand and β-turn secondary structure, in agreement with the recently determined X-ray crystal structure, and that this total β-strand content undergoes a small increase ($\sim$5%) with packaging of RNA. The subunits are relatively deficient in α-helix secondary structure, estimated at <25%, and therefore must contain extensive amounts (>20%) of loops and irregular chain conformations. The Raman spectra also show the following: (1) The molecular environments of as many as four tryptophan residues per subunit are altered upon packaging RNA, resulting in stronger 1N-H hydrogen bonding for two Trp residues and more hydrophobic environments for two indole rings. (2) Hydrogen-bonding states of the seven Tyr residues per subunit do not change detectably when RNA is packaged. At least five tyrosine OH groups are involved exclusively as strong hydrogen bond donors to protein acceptor groups, which suggests restricted access of solvent H_2O molecules to these parahydroxyls. (3) Hydrogen-bonding states of the 14 Cys S-H groups are the same in top, middle, and bottom components. (4) Bands of the ionized carboxyl groups of Asp and Glu are detected in all viral components and no differences occur in these bands with RNA packaging. (5) Significant rearrangement of aliphatic side chains within the viral capsid may occur with packaging of RNA. (6) BPMV middle and bottom components exhibit no detectable differences in subunit secondary structure. A comparison of Raman spectra of crystal and solution states of the BPMV middle component reveals only minor structural differences between the two, and these are restricted almost exclusively to Raman bands of RNA in the region of assigned phosphodiester conformation markers. Although in both the crystal and solution only C3′ endo/anti nucleosides are detected, the crystal exhibits a weaker 813-cm^{-1} band and stronger 870-cm^{-1} band, which suggests that $\sim$8% ($\pm$3% uncertainty) of the nucleotides have O-P-O torsions configured differently in the crystal from that in the solution.

Bean pod mottle virus (BPMV) is a member of the comovirus family. Its virion is characterized by a divided genome and a capsid subunit containing two different polypeptide chains (heterodimer). The two single-stranded RNA molecules are packaged separately in capsids that are composed of identical numbers of heterodimers. Isolation of BPMV from infected plants results in a mixture of the two ribonucleoproteins, as well as empty protein shells. Separation by sucrose gradient sedimentation yields a top component of 54 S [5.0

† Studies of Virus Structure by Laser Raman Spectroscopy: Part 26. Supported by NIH Grants AI11855 (G.J.T.) and AI18764 (J.E.J.).
* Author to whom correspondence should be addressed.
‡ University of Missouri—Kansas City.
§ Purdue University.

0006-2960/90/0429-5018$02.50/0

$\times 10^6$ daltons (Da)], a middle component of 91 S (6.5×10^6 Da of which 2.0×10^6 is RNA), and a bottom component of 112 S (7.5×10^6 Da of which 2.5×10^6 is RNA). The base percent composition of the RNA molecule of the middle component is A:U:G:C 33:31:19:17, while that of the larger RNA molecule of the bottom component is 32:32:21:16 (Bruening, 1977). The amino acid sequences of the two polypeptide chains of the heterodimer have been derived from the sequence of a cDNA transcript of the viral RNA gene (Chen et al., 1989). The polypeptide sequences are largely consistent with amino acid compositions proposed previously (Semancik & Bancroft, 1965).

The salient structural feature that distinguishes the middle and bottom components of BPMV is the size of the viral RNA molecule. The RNA of the bottom component contains 1400 more nucleotides than that of the middle component, mainly greater numbers of G and U residues. It has also been found that the middle component is less stable than the bottom component at alkaline conditions in the presence of chloroform, although all components are stable at neutral pH (Semancik & Bancroft, 1965). Recently, Chen et al. (1989) determined the three-dimensional structure of the BPMV middle component to 3.0-Å resolution by X-ray crystallography and found nearly 20% of the RNA to be clearly visible in the electron density map. Further details of the secondary structure and assembly of the top, middle, and bottom components of BPMV remain to be determined.

In this work we apply laser Raman spectroscopy to investigate structural properties of BPMV in solution and in the crystal state. Previous applications of the Raman method to single-stranded RNA plant viruses and DNA bacteriophages for assessment of macromolecular structures have been reviewed recently (Thomas, 1987). Here, we seek to address the following questions: (i) What differences, if any, exist among the secondary structures of the protein subunits of the top, middle, and bottom components of BPMV? (ii) What amino acid residues may be involved in interactions that differentiate the stability and/or organization of the three components? (iii) What conformations exist for viral RNA backbones and nucleotides of middle and bottom components? (iv) What structural differences, if any, can be recognized between the BPMV virion in aqueous solution and in the crystal? In these and related studies of virus structure by Raman spectroscopy (Thomas, 1987), we hope to identify specific Raman bands that can be used generally to signal molecular interactions between viral constituents.

Experimental Procedures

1. Isolation and Purification of BPMV. BPMV was isolated and purified by extraction from mixtures of chloroform and 1-butanol, using the following procedure (Semancik & Bancroft, 1965). Frozen leaves from inoculated bean plants were ground in a slurry (0.4 g of leaves/mL of solution) of 0.1 M potassium phosphate buffer ($KH_2PO_4 + K_2HPO_4$), pH 7, 0.01 M Na_2EDTA, and 0.4% β-mercaptoethanol and blended to homogeneity. The mixture was centrifuged at 9000 rpm for 25 min and the supernatant, filtered through cheesecloth, was mixed with an equal volume of 1:1 chloroform–butanol solution. After being stirred in the cold for 30 min, the mixture was centrifuged at 8000 rpm for 15 min and the upper aqueous layer was recovered and centrifuged at 9000 rpm for 25 min to pellet the precipitated virus. The pellet was resuspended in 0.1 M phosphate–0.01 M EDTA buffer, pH 7.0, and the suspension was centrifuged at 15000 rpm for 20 min to sediment debris. The supernatant was centrifuged at 30000 rpm for 4 h to pellet the virus, which was again resuspended in the same phosphate–EDTA buffer and repelleted as before. The BPMV pellet so obtained consists of a highly purified but unresolved mixture of top, middle, and bottom components.

The purified virus pellet was centrifuged at 39000 rpm for 18 h in a 4% CsCl gradient to separate four bands corresponding to (i) top, (ii) middle, (iii) bottom upper, and (iv) bottom lower components. The four components were collected and on the basis of their absorption coefficients ($\epsilon_{260} \times 10^3 = 1.2, 8.1, 8.1$ and 8.1 and $A_{260}/A_{280} = 0.70, 1.73, 1.79$ and 1.79 for i–iv, respectively) were diluted to final concentrations of approximately 10 mg/mL in the above phosphate–EDTA buffer. Each solution was centrifuged at 42000 rpm for 4 h to yield a pellet. Finally, each pellet was resuspended in phosphate–EDTA buffer, to a concentration of approximately 10 mg/mL. BPMV crystals were the same specimens examined by X-ray crystallography (Chen et al., 1989).

2. Sample Handling for Raman Spectroscopy. The virus or capsid solution (~ 150 μL), as prepared above, was centrifuged at 35000 rpm for 3 h in a Beckman airfuge and the pellet was resuspended in the appropriate volume of the above phosphate–EDTA buffer (pH 7) to a final concentration of 100 μg/μL. Approximately 10 μL of this solution was sealed in a Raman capillary cell (Kimax No. 34507) and thermostated at 8 ± 0.5 C while the spectrum was obtained (Thomas & Barylski, 1970).

Raman spectra were excited with the 514.5-nm line of a Coherent Innova 70 argon ion laser, using approximately 100 mW of radiant power at the sample, and were recorded on a Spex Ramalog 1401 spectrometer under the control of a North Star Horizon II microcomputer (Li et al., 1981). Data were collected with a spectral slit width of 8 cm^{-1} at increments of 1 cm^{-1} and integration time of 1.5 s. Seven scans were averaged for the region 300–1800 cm^{-1} and 35 scans for the regions 600–900 cm^{-1} and 2500–2600 cm^{-1}.

3. Data Analysis. Solvent and scattering backgrounds were subtracted from the signal-averaged spectra by difference methods described elsewhere (Verduin et al., 1984). However, in order to avoid the compounding of spectral noise that occurs in successive substractions of spectra, the solvent background was not usually subtracted from pairs of spectra used in subsequent subtractions, such as the spectra of middle and bottom components, which are compared by subtraction below. On the other hand, when nonidentical buffers were employed, such as in the case of the crystalline and solution forms of the BPMV middle component, it was necessary to subtract the respective buffers prior to comparing the virus Raman spectra by subsequent subtraction.

For computation of difference spectra, intensities were normalized arbitrarily to minimize differences for bands that are believed invariant to the difference(s). In practice this was equivalent to normalization either to the Raman band near 1005 cm^{-1} due to phenylalanine residues (phenyl ring vibration), to the 1457-cm^{-1} band of side-chain methylene groups (CH_2 scissoring), or to the 1100-cm^{-1} band of RNA phosphates (PO_2^- symmetric stretching). In the difference spectra, peaks that are less than 2-fold more intense than the base-line noise level are considered to be nonsignificant. Deconvolution procedures were carried out on an IBM PS/2 microcomputer with an installed numeric data processor using software developed in our laboratory and described elsewhere (Thomas & Agard, 1984).

Results

Raman spectra in the region 400–1800 cm^{-1} of three re-

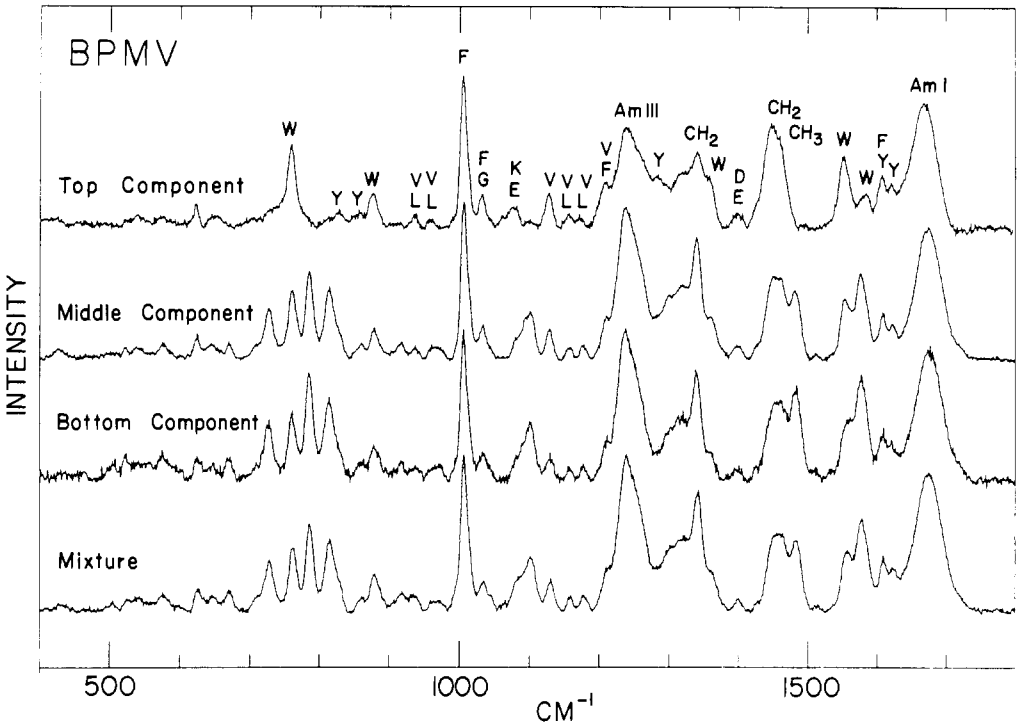

FIGURE 1: Raman spectra in the region 400–1800 cm^{-1} of BPMV components in solution (0.1 M KH_2PO_4–0.01 M EDTA, pH 7.0 buffer) at 8 °C. From top to bottom: BPMV capsid (top component); BPMV virion containing smaller RNA molecule (middle component); BPMV virion containing larger RNA molecule (bottom component); unseparated mixture of top, middle, and bottom components. Labels in the spectrum of the top component indicate amino acid assignments. Bands present in middle and bottom components, but absent from the top component, are due to RNA groups. Detailed frequencies and assignments are given in Table I. See also Figure 2.

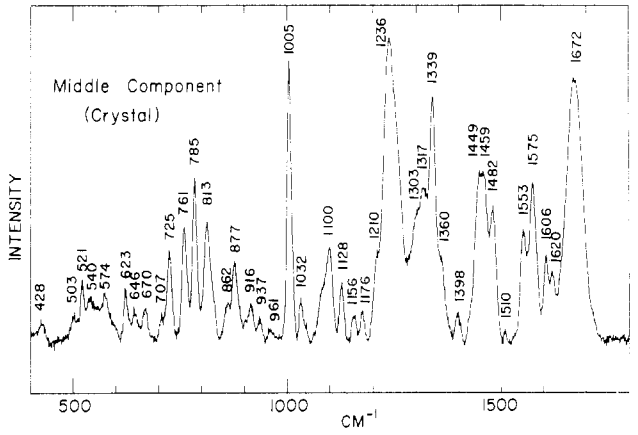

FIGURE 2: Raman spectrum in the region 400–1800 cm^{-1} of a single crystal of BPMV middle component suspended in mother liquor (Chen et al., 1989) at 8 °C. The spectrum was compensated for the weak Raman scattering of the mother liquor.

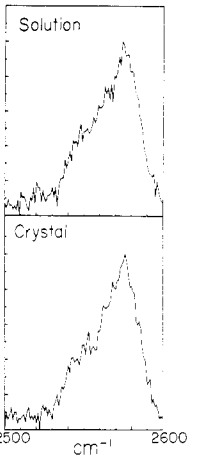

FIGURE 3: Raman spectra in the region 2500–2600 cm^{-1} of the BPMV middle-component crystal (bottom) and solution (top).

solved components of BPMV, the top (empty capsid), middle (light ribonucleoprotein), and bottom (heavy ribonucleoprotein) isolates, are shown in Figure 1. For comparison, the Raman spectrum of the homogeneous mixture of these isolates (see Experimental Procedures) is also shown in Figure 1. In Figure 2, we show the Raman spectrum of the crystal of the BPMV middle component, for which the 3.0 Å resolution X-ray structure was recently determined (Chen et al., 1989). We have also examined the Raman spectra of BPMV components in the region 2500–2650 cm^{-1}, where cysteine sulfhydryl groups give characteristic bands due to the SH stretching vibration (Thomas, 1987). These data for middle-component crystal and solution are shown in Figure 3. Difference spectra showing comparisons of data for different BPMV components are given in Figures 4–8.

A comprehensive tabulation of Raman band frequencies with residue assignments for major peaks and discernible shoulders in the spectra of top and middle components is given in Table I. Raman bands that are particularly sensitive to small differences in protein structure or to protein–RNA interactions do not exhibit identical frequencies and intensities in spectra of the different particles. Examples are the amide I and amide III bands (Table II) and indole ring modes of the tryptophan residues (Table III).

Discussion

1. Secondary Structure of the Capsid Subunit. The Raman amide I and amide III bands of the top component (Figure 1) are centered near 1670 ± 2 and 1237 ± 2 cm^{-1}, respectively, indicating β-sheet as the predominant secondary structure of the capsid subunit (Chen & Lord, 1974; Sargent et al., 1988). The amide I and III profiles of Figure 1 are qualitatively and quantitatively similar to those obtained for the tailspike protein of bacteriophage P22 (Sargent et al., 1988), from which it may

Table I: BPMV Raman Frequencies, Relative Intensities, and Assignments[a]

capsid[b]	virion[c]	assignments[d]
	426 (0.6)	skeletal; ribose
	520 (0.7)	skeletal: Ade
539 (0.8)	537 (0.7)	skeletal; Ade
576 (0.7)	574 (0.8)	ribose
623 (1.5)	622 (1.7)	Phe
650 (0.7)	643 (1.0)	Tyr; ribose
	669 (0.9)	Gua
706 (0.5)	707 (0.8 S)	Met; ribose
	725 (2.7)	Ade
760 (5.5)	759 (3.9)	Trp; ribose
	784 (5.3)	Cyt, Ura
	813 (4.5)	O–P–O str
828 (0.9)	829 (1.8 S)	Tyr
856 (0.5)	859 (1.0)	Tyr; ribose
880 (2.3)	877 (1.9)	Trp; ribose
913 (0.2)	916 (1.1)	Ala; ribose
937 (0.6)	936 (0.9)	Val, Leu (CH_3 sym rock)
960 (0.6)	967 (0.8)	Val, Leu (CH_3 sym rock); ribose
1005 (10.0)	1005 (9.7)	Phe; ribose
1032 (2.2)	1032 (1.4)	Phe; Gua; ribose
1078 (1.4 S)	1079 (1.3 S)	Thr
1099 (0.4)	1100 (3.0)	PO_2^- str; Ala
1128 (2.3)	1127 (2.0)	Val (C–C str)
1157 (1.0)	1156 (0.8)	Val, Leu (CH_3 sym rock, ip); ribose
1173 (0.6)	1176 (0.8)	Val, Leu (CH_3 asym rock, op); ribose
1210 (3.0)	1209 (2.8)	Phe, Tyr
1236 (6.6 B)	1237 (10.0 B)	amide III; Ura, Cyt
1265 (4.5 S)	1266 (5.5 S)	amide III, His, Tyr
1284 (3.3 S)		amide III, His
1296 (2.8 S)	1300 (4.2 S)	Ade; Cyt
1319 (3.7 S)	1318 (4.9 S)	CH_2 twist/wag, CH def; Gua
1340 (5.1)	1339 (7.9)	CH_2 twist/wag, Trp; Ade, Gua
1359 (3.5 S)	1359 (2.8 S)	Trp
1399 (0.9)	1398 (0.8)	CO_2^-
1450 (6.7)	1449 (5.4)	CH_2 scissor
1463 (5.4 S)	1460 (5.4 S)	CH_3 asym def, CH_2 scissor; ribose
	1480 (4.5)	Gua, Ade
	1511 (0.4)	Ade
1553 (4.8)	1552 (4.0)	Trp
1584 (2.4)	1574 (5.6)	Trp; Gua, Ade
1607 (3.5)	1606 (3.1)	Phe, Tyr
1621 (2.9)	1620 (2.4)	Tyr
1669 (8.3 B)	1672 (8.7 B)	Amide I; Ura, Gua (C=O)
2549 (4.5 S)	2549 (4.7 S)	Cys (SH str)
2575 (10.0)	2575 (10.0)	Cys (SH str)

[a] Frequencies (cm^{-1}) are accurate to ±2 cm^{-1}; relative intensities (in parentheses) are on an arbitrary 0–10 scale, with 10 assigned to the strongest band in each spectrum. S and B indicate unresolved shoulder and broad band, respectively. [b] From capsid solution spectrum of Figure 1. [c] From middle-component solution spectrum of Figure 1. [d] Standard abbreviations are given for protein and RNA residues and chemical subgroups. Where multiple assignments are given, the major contributor(s) is(are) given first. See also the discussion in text.

Table II: Conformation-Sensitive Amide I and Amide III Raman Bands of BPMV Components[a]

BPMV component	amide I frequency (cm^{-1})	amide I intensity (I_{1672}/I_{1005})	amide III frequency (cm^{-1})	amide III intensity (I_{1236}/I_{1005})
top	1669	0.83	1236	0.66
middle	1672	0.87	1237	1.03
bottom	1673	0.92	1238	1.06
mixture	1673	0.89	1238	1.01
crystal	1672	0.94	1238	1.08

[a] From data of Figure 1. Amide intensities were determined by the peak height method, using a base-line tangent to the wings of the amide band. A similar procedure was used for the reference (1005 cm^{-1}) band intensity.

be concluded that the secondary structure of the BPMV subunit contains ~50% β-sheet. In order to derive a semiquantitative estimate of the β-structure content of the capsid

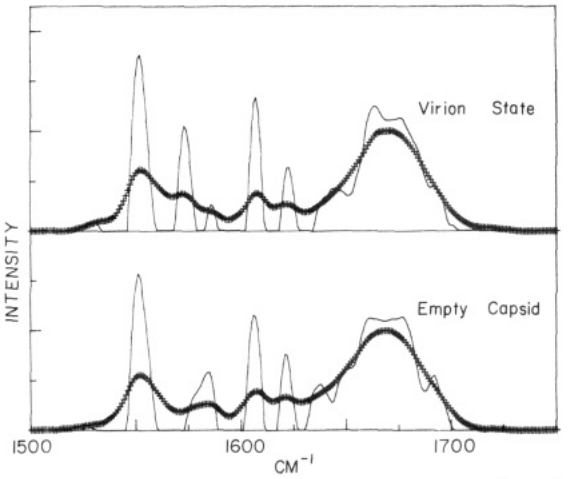

FIGURE 4: Raman spectra in the region 1500–1750 cm^{-1} (++) of proteins of the BPMV middle and top components, each compared with their Fourier deconvolutions (—). Upper panel: The spectrum of the middle component protein was obtained by subtracting the spectrum of BPMV RNA from the Figure 1 spectrum of the middle component. Lower panel: Spectrum of top component from Figure 1. Deconvolutions were obtained by use of a Gauss–Lorentz deblurring function of 20-cm^{-1} half-width.

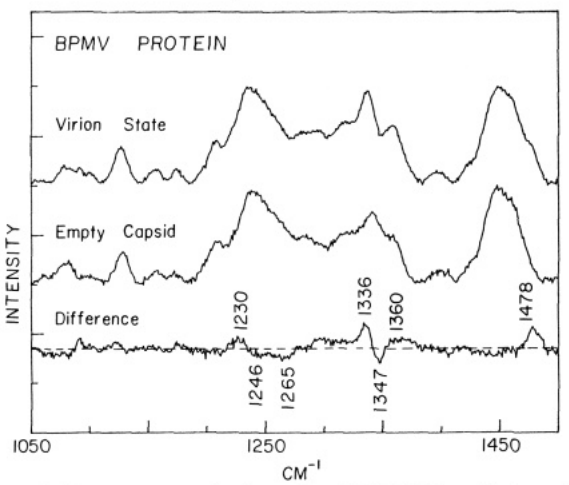

FIGURE 5: Raman spectra in the region 1100–1500 cm^{-1} of proteins of the BPMV middle and top components, and their difference spectrum. The spectrum of the middle-component protein (upper trace) was obtained as described in the Figure 4 legend. The spectrum of the top component (center trace) is from Figure 1. The difference spectrum (lower trace) was computed so as to minimize difference intensities of bands of hydrocarbon side chains at 1125 (C–C stretching) and 1460 cm^{-1} (CH_2 scissoring).

Table III: Conformation-Sensitive Raman Bands of the Tryptophan Residues of BPMV Particles and Probable Conformational States

virus component	frequency σ_{17} (cm^{-1})	average hydrogen bonding of indole 1NH[a]
top	880	weak
middle (crystal)	877	moderate
middle	877	moderate
bottom	879	moderate
mixture	879	moderate

[a] Based upon correlations established by Miura et al. (1988).

subunit, we have applied Fourier deconvolution to the amide I and III band profiles (Thomas, 1985). The results for amide I are shown in Figure 4. The amide band intensity distributions resolved by deconvolution suggest that the capsid subunit contains 50 ± 5% β-strand and 20 ± 5% α-helix. The remaining secondary structure (~30%) is ascribed to loops and

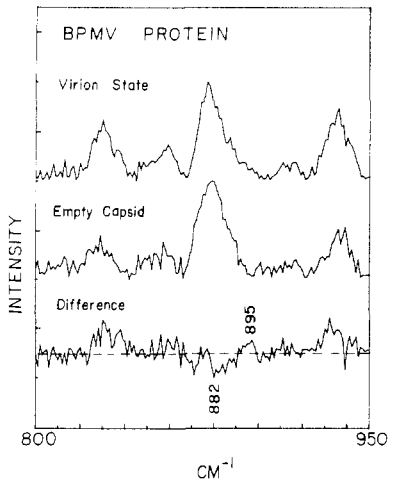

FIGURE 6: Raman spectra in the region 800–950 cm^{-1} of proteins of the BPMV middle and top components, and their difference spectrum. The spectrum of the middle-component protein (upper trace) was obtained as described in the Figure 4 legend. The spectrum of the top component (center trace) is from Figure 1. The difference spectrum (lower trace) was computed so as to minimize the net intensity difference of the composite tryptophan band between 860 and 900 cm^{-1}.

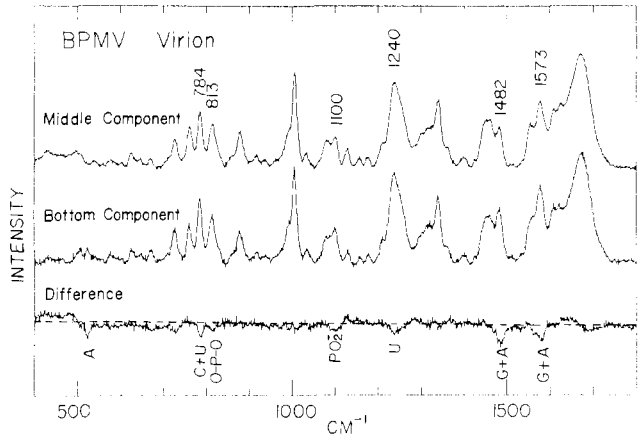

FIGURE 7: Raman spectra in the region 400–1800 cm^{-1} of BPMV middle and bottom components, and their difference spectrum. From top to bottom: BPMV middle component from Figure 1; BPMV bottom component from Figure 1; difference spectrum (middle component minus bottom component).

irregular conformations. It should be noted that the Raman amide I and amide III markers are sensitive primarily to peptide group torsions (ϕ, ψ) and C=O and N—H hydrogen bonding. Therefore, residues in extended turns or loops with peptide geometry and/or hydrogen bonding similar to those in β-sheet domains are also expected to contribute to the total β-strand content measured by Raman spectroscopy. The Raman determination of 50 ± 5% β-strand may therefore include a significant number of residues in reverse turns and is not inconsistent with the β-sheet (~40%) plus turns (~10–15%) secondary structure determined by X-ray crystallography.

Raman amide profiles observed for middle and bottom components are similar to those of the capsid (Figure 1 and Table II). However, for the ribonucloproteins, interpretation of the amide bands is complicated by overlap from bands of the packaged RNA. In a previous study of belladonna mottle virus (BDMV) (Prescott et al., 1985), difference Raman spectroscopy was employed to compensate for the overlapping Raman bands of the RNA. Use of the same procedure here (Figure 5) indicates that minor changes occur in the secondary structure of BPMV subunits as a consequence of RNA packaging in the virion. The positive band near 1230 cm^{-1} and the negative bands near 1248–1260 cm^{-1} in the difference spectrum (bottom) of Figure 5 indicate a small but significant increase of subunit β-strand content at the expense of disordered structure. This is supported by Fourier deconvolution results (Figure 4), which show a small but definitive change in the amide I band contour near 1670 cm^{-1}, suggesting that disordered segments of the subunit polypeptide chain in the capsid may form β-strand structure as a consequence of RNA packaging. We estimate that ~5% of the subunit secondary structure is affected by RNA packaging.

2. Side-Chain Interactions and Environment. (a) Tyrosine. There are seven tyrosines per heterodimer (subunit), and each contributes to the characteristic Raman bands of the phenolic ring at 642, 858, 1210, 1260, and 1620 cm^{-1} (Table I). Lord and co-workers (Siamwiza et al., 1975) have shown that the relative intensity of the bands at 858 and 829 cm^{-1} (I_{858}/I_{829}) is diagnostic of the hydrogen-bonding state of the phenolic OH group. When OH is the acceptor of a strong hydrogen bond from a positive donor group, it is observed that I_{858}/I_{829} = 2.50 (A state). Tyrosines exclusively in the A state are found in coat subunits of Pf1 and fd virions (Thomas et al., 1983). When the phenolic OH acts as both donor and acceptor of moderately strong hydrogen bonds, as for example when exposed to solvent H_2O molecules or otherwise hydrogen bonded to both donor and acceptor groups, then I_{858}/I_{829} = 1.25 (E

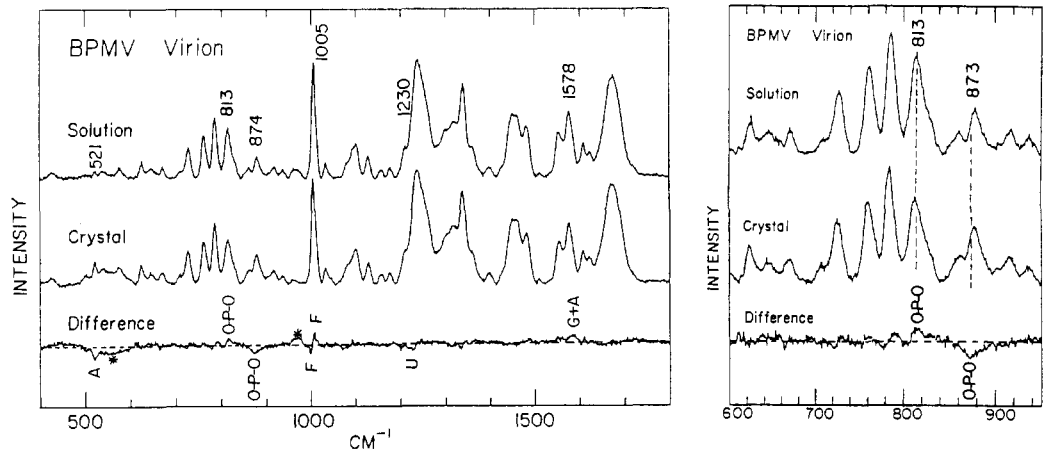

FIGURE 8: Left panel: Raman spectra in the region 400–1800 cm^{-1} of the BPMV middle component in solution (upper trace) and crystal (center trace), and their difference spectrum (lower trace). Bands near 550 and 970 cm^{-1}, marked with asterisk, are due to base-line artifacts. Right panel: Expansion of the spectral region 600–950 cm^{-1}.

state). Tyrosines exposed at the protein–solvent interface usually exist in the E state (Thomas et al., 1986). Finally, when OH is the donor of a strong hydrogen bond to a negative acceptor group, $I_{858}/I_{829} = 0.30$ (D state). Tyrosines in the D state have been identified previously in subunits of several RNA plant viruses (Verduin et al., 1984, Prescott et al., 1985).

From the data of Figure 1, we find for the top component $I_{858}/I_{829} = 0.50 \pm 0.10$. Since the Raman bands monitor all tyrosines, the intensity quotient of 0.50 represents an average over hydrogen-bonding states of seven Tyr residues per subunit. The deviation of ±0.10 represents the uncertainty in the base line employed for measurement of peak heights in this spectral region. There are two possible configurations of the seven tyrosines that are consistent with $I_{858}/I_{829} = 0.50 \pm 0.10$: viz., the distributions E = 2, A = 0, D = 5, and E = 1, A = 0, D = 6, for which the calculated quotients are 0.57 and 0.44, respectively. We conclude that in the capsid no tyrosine exists solely as a strong hydrogen bond acceptor, and the majority exist as strong hydrogen bond donors. This conclusion implies either that few tyrosines are located at the protein surface for hydrogen bonding with solvent H_2O molecules or that if tyrosines do exist at the surface they are preempted from assuming the E state and are involved exclusively as hydrogen bond donors to appropriate acceptors. In this respect, the tyrosines of the BPMV capsid are similar to those in capsids of RNA plant viruses examined previously (Verduin et al., 1984; Prescott et al., 1985).

The middle and bottom components exhibit a strong Raman line from RNA near 813 cm^{-1}, which largely obscures the 829-cm^{-1} component of the tyrosine doublet and precludes direct measurement of the I_{859}/I_{829} intensity ratio in these ribonucleoproteins. In order to extract the intensity of the 829-cm^{-1} band from the spectrum of the middle component, we subtracted the RNA contribution estimated from the known BPMV RNA spectrum in the 800–900-cm^{-1} region (Figure 6). The intensity ratio I_{859}/I_{829} of the BPMV middle component determined in this manner is 0.55, which is within experimental uncertainty of the value observed for the top component. The same result can be inferred from the difference spectrum of the bottom component (Figure 7). Therefore, we conclude that the seven Tyr residues per subunit have the same molecular environments in the empty capsid and in both BPMV ribonucleoproteins. These results indicate that packaging of RNA has virtually no effect upon the hydrogen-bonding environments of subunit tyrosine residues. The absence of Raman intensities in the region 820–860 cm^{-1} of the difference spectrum of Figure 8 suggests that the hydrogen-bonding environments of subunit tyrosine residues are also invariant to the solution-to-crystal transformation of BPMV.

(*b*) *Tryptophan.* Raman spectra of all samples (Figure 1) display bands near 760, 880, 1340, 1360, and 1554 cm^{-1}, which are assigned (Table I) to the 16 tryptophan residues per BPMV subunit (Chen et al., 1989). Of these, the bands at 880 and 1360 cm^{-1} are dependent on the tryptophan environment (Yu, 1974; Kitagawa et al., 1979; Harada et al., 1986). The Raman band at 1360 cm^{-1} has been assigned to the high-frequency component of a Fermi doublet involving an indole ring skeletal stretching fundamental (σ_7) and a combination vibration (Harada et al., 1986). The 880-cm^{-1} frequency has been assigned to an indole ring mode involving both ring stretching and exocyclic 1N–H in-plane bending (Takeuchi & Harada, 1986).

Recently, quantitative correlations have been established between Raman bands of the indole ring and the molecular environment of the tryptophan side chain (Miura et al., 1988). When the indole ring is inaccessible to solvent and sequestered in a hydrophobic pocket, the 1360-cm^{-1} band is sharp and relatively intense. On the other hand, solvent contact or other hydrophilic exposure of the tryptophan residue results in a dramatic decrease in the intensity of the 1360-cm^{-1} band. In such a case, the 1360-cm^{-1} band may completely elude direct detection because of the superposed stronger Raman bands of other protein residues. To complement the information contained in the 1360-cm^{-1} band, the strength of hydrogen bonding by the indole 1N–H donor can be monitored through the position of the σ_7 band: Very weak 1N–H hydrogen bonding leads to a band center near 882 cm^{-1}, while very strong hydrogen bonding causes the band center to shift to 872 cm^{-1}. Moderate hydrogen bonding, as often occurs for solvent-exposed indole rings in proteins, generates the σ_7 band center near 877 cm^{-1} (Miura et al., 1988).

The Raman bands of BPMV at 880 and 1360 cm^{-1} (Figure 1) reflect the average molecular environment of the 16 tryptophan residues per subunit and indicate moderately strong hydrogen bonding for the majority of these in both capsid and nucleoprotein particles. However, small differences are evident between capsid and virion. The higher relative intensity of the virion 1360-cm^{-1} band (Figure 5) is consistent with two (±one) Trp residues of the virion existing in a more hydrophobic environment than that of the capsid. The lower relative intensity of the virion 882-cm^{-1} band (Figure 6) indicates that two (±one) Trp residues also form stronger 1N–H hydrogen bonds in the virion than in the capsid (Table III). Therefore, environments of as many as four Trp residues may be altered by RNA packaging. Since the X-ray structure of the BPMV middle component (Chen et al., 1989) reveals no Trp residues close to the RNA-binding pocket, hydrogen-bonding changes could not involve RNA directly, but could result from small differences in protein side-chain interactions or differences in tryptophan–H_2O interactions between capsid and virion.

Another possible explanation for the negative 882 cm^{-1} band in the Figure 6 difference spectrum (as well as for the positive difference band at 895 cm^{-1}) is that the RNA conformation in the virion differs slightly from that of the protein-free BDMV RNA employed for the difference spectrum calculation. However, this would not explain the observed intensity change at 1360 cm^{-1}, where no RNA contribution occurs. Our results suggest more probably that packaging of RNA indirectly alters the environments of a few of the Trp residues per subunit.

(*c*) *Cysteine.* Cysteine residues of capsid subunits are the only contributors to the interval 2500–2600 cm^{-1} in the Raman spectrum of an RNA virus and the bands are unequivocally assigned to cysteinyl S–H stretching vibrations (Thomas et al., 1976). The characteristic SH Raman band from cysteine side chains is usually centered near 2575 cm^{-1}, although dependency of the band position and intensity upon factors that may change the capsid assembly state have been noted (Verduin et al., 1984; Thomas, 1987). Strongly hydrogen bonded SH groups (e.g., those donating hydrogen bonds to C=O acceptors) exhibit a significantly broader SH Raman band near 2550 cm^{-1} (H. Li and G. J. Thomas, Jr., unpublished results). FTIR studies of cysteine interactions in hemoglobin have yielded similar results (Bare et al., 1975). Figure 3 shows the 2500–2600-cm^{-1} region of the Raman spectrum of the BPMV middle component. For both solution and crystal we observe the main SH band at 2575 cm^{-1} and a shoulder near 2550 cm^{-1}. Similar profiles (data not shown) are observed for top and bottom components, indicating similar SH hydrogen-bonding environments in all BPMV components. The

band intensity ratio, $I_{2550}/I_{2575} \approx 0.5$, indicating a 1:2 ratio of strong to weak SH hydrogen bond donor groups. We also conclude from the data of Figure 3 that the nature of SH hydrogen bonding is invariant to crystallization of the middle component.

(*d*) *Aspartate and Glutamate.* The prominent Raman band at 1400 cm^{-1} in all spectra (Figure 1) confirms the ionization of side-chain carboxyls (COO^-) of aspartate and glutamate residues at neutral pH. The absence of a band between 1725 and 1750 cm^{-1} shows that a significant population of protonated carboxyl groups (COOH) is not present in any BPMV components at conditions believed relevant to normal virus assembly. Similar results were obtained for the middle component in the range $6.9 < pH < 9.1$.

(*e*) *Aliphatic Side Chains.* The positive intensity at 1336 cm^{-1} and negative intensity at 1347 cm^{-1} in the difference spectrum of Figure 5 suggest that aliphatic amino acid side chains assume different configurations in capsid and virion. The configurational changes may result directly or indirectly from RNA packaging. The positive difference band at 1478 cm^{-1} may also result in part from aliphatic amino acid side chains, but is more likely due to uncompensated RNA intensity at this frequency. The RNA contribution is discussed in section 5.

3. Structural Comparison between RNA of Middle and Bottom Components. Figure 7 shows the difference spectrum obtained by subtracting the spectrum of the bottom component (subtrahend) from that of the middle component (minuend), using the protein 1005-cm^{-1} band as the normalization basis. The Raman bands at 1005 and 1457 cm^{-1}, due respectively to phenylalanine and CH_2 groups, are both perfectly compensated in the difference spectrum. Most other protein contributions to the spectra are also well compensated by this method of difference computation. Since the bottom component contains a larger RNA molecular mass, compensation on the basis of the protein band intensities will result in a difference spectrum with conspicuous negative bands assignable to the RNA. It is clear from Figure 7 that this is indeed the case. Thus, the negative peaks at 521 (A), 784 (C + U), 813 [backbone (bk)], 1100 (bk), 1240 (U), 1482 (G + A) and 1573 cm^{-1} (G + A) are all due to the excess RNA of the bottom component. Specific assignments to base (A, C, G, U) and backbone contributors are indicated in Figure 7. The intensities observed in the difference spectrum reflect the fact that the bottom-component RNA differs from the middle-component RNA mainly in its greater mole percentages of U (13.6%) and G (8%). (The positive difference band, centered near 1645 cm^{-1} is attributed to water, which is not fully compensated in this subtraction, since the two solutions of virus particles contain slightly different solute concentrations.) It is evident from Figure 7 that no significant differences occur between subunit conformations in middle and bottom components. In particular, all of the intensity differences in the intervals 1630–1680 and 1230–1300 cm^{-1} may be rationalized in terms of the contributions from the RNA bases (1240 and 1672 cm^{-1}) and from solvent H_2O molecules (broad band at ca. 1645 cm^{-1}). No Raman amide band intensity differences can be identified in this difference spectrum. The intensity ratio of RNA backbone markers observed here (I_{813}/I_{1100} = 1.45 in both particles) is similar to ratios observed for other ssRNA plant viruses (Verduin et al., 1984; Prescott et al., 1985; Thomas, 1987).

For both middle and bottom components the intensity ratio of Raman bands from phosphodiester and phosphodioxy group vibrations (I_{813}/I_{1100}) is 1.45 ± 0.05, indicating 88 ± 3% of nucleotides in the A-form gauche/gauche (g^-,g^-) phosphodiester geometry for both components (Thomas & Hartman, 1973). Figure 7 also shows a 23 ± 3% intensity difference between the phophodioxy Raman band (1100 cm^{-1}) in bottom and middle components, which is in quantitative agreement with the RNA mass difference (25%) between these two ribonucleoprotein particles.

Table IV: Raman Bands Sensitive to Physical States of the BPMV Middle Component[a]

frequency (cm^{-1})	intensity	assignment	frequency (cm^{-1})	intensity	assignment
522	–	Ade	1007	+	Phe
813	+	O–P–O	1228	–	Ura, Cyt
874	–	O–P–O	1585	+	Ade, Gua
1000	–	Phe			

[a] The Raman bands listed are those appearing in the difference spectrum of Figure 8 (BPMV middle-component solution minus crystal). Positive sign indicates a band of greater intensity in the solution spectrum; negative sign indicates lower intensity in the solution spectrum.

4. Comparison of Crystal and Solution States of the Middle Component. Figure 2 shows the Raman spectrum of the BPMV middle-component crystal. We have compared this crystal spectrum with that of the middle component in solution (Figure 1) by computing the difference spectrum (solution minus crystal) shown in Figure 8. The absence of significant difference bands through most of the spectral region 400–1800 cm^{-1} demonstrates the absence of large structural differences between crystal and solution. However, a few significant difference bands are detected in the region of RNA phosphodiester vibrations, and these are shown on an expanded scale in the right panel of Figure 8 and are tabulated in Table IV. We interpret these results as follows.

The middle-component crystal yields a Raman intensity ratio I_{813}/I_{1100} = 1.29 ± 0.05, corresponding to 78 ± 3% of the viral RNA phosphate groups in the A-type phosphodiester conformation, which is significantly lower than the value of 1.45 observed for BPMV solutions (above). The only candidate for replacement of the 813-cm^{-1} intensity in the crystal is the enhanced intensity near 870–875 cm^{-1}, which appears as a negative feature in the difference spectrum and indicates that ~8% of the sugar phosphate residues of RNA are configured differently in the solution and crystal. Other minor intensity differences are apparent in bands due to bases at 522 (A), 1228 (U), and 1575 cm^{-1} (G, A) (Lord & Thomas, 1967; Benevides et al., 1988) and may be attributed to base-stacking differences. The positive difference band at 1575 cm^{-1} and the negative difference band at 1228 cm^{-1} are consistent with greater stacking of purines and less stacking of pyrimidines in the crystal structure (Small & Peticolas, 1971; Thomas et al., 1971). We note particularly that the difference spectrum lacks any significant intensity from viral protein in the regions of conformation-sensitive amide I (1630–1680 cm^{-1}) and amide III (1230–1300 cm^{-1}) bands, indicating that the protein secondary structure is invariant to crystallization. The 522-cm^{-1} band is not assignable to S–S groups, since no disulfides are apparent in the crystal structure (Chen et al., 1989) and since Figure 3 shows no evidence that cysteine sulfhydryls are altered between crystal and solution.

The only significant feature in the difference spectrum of Figure 8 that can be assigned to the protein is the pair of negative and positive lobes near 1005 cm^{-1}, reflecting a shift of ~7% of the intensity of the strong and sharp phenylalanine band and corresponding to ~2 of the 30 Phe residues per subunit. Sensitivity of the phenylalanine band to subtle

changes in molecular environment has been observed in other RNA and DNA viruses (Thomas et al, 1983; Verduin et al., 1984), but there is no established structural basis for interpreting the intensity change. Since the crystal structure reveals no surface phenylalanines that are candidates for interaction with RNA (Chen et al., 1989), we speculate that the change does not result directly from differences between RNA packaging in crystal and solution.

5. Comparison of BPMV RNA in Virion and Protein-Free States. As noted in section 2e, the computed difference spectrum of Figure 5 (bottom trace) gives evidence of an incompletely compensated RNA band near 1478 cm^{-1}. Efforts to eliminate this band by amplifying the RNA intensity subtracted from the spectrum of the middle component lead to large spurious features in the difference spectrum. This suggests that the band does not result from undercompensation, but arises from an actual intensity difference between packaged and naked RNA. A band at 1478 cm^{-1} is associated with A- and G-ring vibrations and is sensitive to interactions involving the 7N purine site (Nishimura et al., 1986). The band is expected to be strong in the absence of specific hydrogen bonding to purine 7N groups, and weak (i.e., replaced by a band at ca. 1490 cm^{-1}) when hydrogen bond donation to 7N occurs. Our results indicate that the 1478-cm^{-1} band exhibits greater intensity in the packaged RNA than in protein-free RNA, which implies that RNA packaging may disrupt 7N purine interactions associated with the tertiary structure of the folded protein-free RNA molecule. Presumably, compensating 7N interactions do not occur when the RNA is packaged in the virion. Our data (Figure 5) do not indicate, however, a significant negative difference band at 1490 cm^{-1}, as would be expected for this model. An alternative explanation for the 1478-cm^{-1} difference band is that greater Raman hypochromism (i.e., greater purine base stacking) prevails in naked RNA than in packaged RNA.

Conclusions

The Raman spectra of aqueous solutions of BPMV ribonucleoproteins have been compared with spectra of capsid and protein-free BPMV RNA to resolve conformation-sensitive bands of the viral protein and RNA. The small spectral differences observed between middle and bottom components can be rationalized completely in terms of the primary compositions of their respective RNA molecules. We conclude that viral protein conformations, RNA secondary structures, and possible protein–RNA interactions are similar for middle and bottom components in the solution state. On the other hand, we have observed small but significant spectral differences between BPMV ribonucleoproteins and capsid, which are interpreted as conformational differences between their respective subunits. Specifically, we find that although β-strand is the dominant secondary structure in both empty and RNA-filled capsids, in accordance with the X-ray crystal structure of the middle component (Chen et al., 1989), a nominally greater β-strand content ($\sim$5%) exists for subunits of the virion than for those of the empty capsid. This finding suggests that a small conformation change could be associated with packaging (or release) of the viral genome. The X-ray diffraction data of Chen et al. (1989) show that the outer structure of the protein shell is unchanged in the three different components of BPMV. Indeed, it is possible to cocrystallize all three components in the same crystal, and this crystal diffracts to at least 3-Å resolution. At present only the middle-component crystal has been refined, so it is the only structure known accurately in its entirety. However, on the basis of a partial data set obtained from crystals of empty capsids it can be concluded that 23 amino acid acids at tne N terminus of the large protein are in different positions in the empty capsid and middle component (J. E. Johnson, unpublished results). It is not yet clear if these residues are spatially disordered in the empty capsid, or ordered but in different positions. If these residues were disordered in the empty capsid, then the middle component would have roughly 5% more secondary structure than the empty capsid, in agreement with the Raman spectra.

The Raman spectra of single crystals of the BPMV virion (middle component) and capsid were also investigated and compared with the corresponding spectra obtained from solution samples. The Raman spectra indicate no major changes in either capsid or virion proteins as a result of crystallization. Similarly, the RNA molecule of the virion assumes a highly ordered A-type secondary structure with C3′ endo/anti nucleoside conformations in both crystal and solution states of the middle component. However, the 813-cm^{-1} Raman band, which is assignable to the RNA backbone and which is the most sensitive to ordered (g^-,g^-) phosphodiester conformers, is 8% more intense for the solution than for the crystal of the BPMV middle component. The crystal, on the other hand, displays a band at 870 cm^{-1}, assignable to RNA and of greater intensity than the corresponding band of the solution spectrum. (See Figure 8 difference spectrum.) We interpret this as an indication that approximately 8% of the nucleotide residues of the packaged RNA molecule are configured differently in the crystal (870-cm^{-1} marker) than in the solution (813-cm^{-1} marker). In studies of DNA, the 870-cm^{-1} band has been assigned to phosphodiester conformations (torsion angles $\beta \approx 180$, $\gamma \approx 180$) associated with C-type secondary structure (Nishimura & Tsuboi, 1986). Consistent small differences between crystal and solution are also observed in other RNA bands that are sensitive primarily to base stacking.

Since segments of the packaged RNA identified in the electron density map as icosahedrally ordered and tethered to the capsid wall at its 3-fold vertices (Chen et al., 1989) are not expected to differ between crystal and solution, we attribute the observed conformational differences to the remaining 80% or so of the packaged RNA molecule that is spatially disordered and not visualized in the crystal structure. Although spatially disordered, the nonbound RNA segments are shown by the Raman spectrum to contain a majority (58%) of nucleotides with the A-form (g^-,g^-) phosphodiester geometry. The Raman data do not permit a more detailed description of which RNA residues may be affected differently by crystal and solution environments.

Packaging the RNA molecule in BPMV also elicits structural changes of selected amino acid side chains of the subunits. Although tyrosines are unaffected, we find increases in tryptophan hydrogen bond donation (indole 1N–H) and less exposure of tryptophan to hydrophilic environments when RNA is packaged. Relatively strong hydrogen bonding is observed for $^1/_3$ of the cysteine sulfhydryls (to C=O acceptors) in the middle-component solution and crystal. Although preliminary results indicate no significant difference in the nature of S–H bonding for the empty capsid, further studies are planned to investigate whether RNA groups serve as acceptors for cysteine S–H interactions in the middle component.

BPMV contains similar amounts of subunit β-strand structure and similar amounts of ordered A-type RNA secondary structure, as do other ssRNA plant and bacterial viruses (Hartman et al., 1973; Thomas et al., 1976; Verduin et al., 1984; Prescott et al., 1985; Thomas, 1987). Raman bands identified in this work, which signal RNA packaging and

which may reflect direct or indirect RNA–protein interactions in the virion, are summarized in Table IV. Additional experiments are required to determine whether the observed small differences in RNA band intensities between the solution and crystal states of middle component are due to different RNA packaging motifs or differences in RNA–protein interactions.

References

Bare, G. H., Alben, J. O., & Bromberg, P. A. (1975) *Biochemistry 14*, 1578–1583.

Benevides, J. M., Wang, A. H.-J., van der Marel, G. A., van Boom, J. H., & Thomas, G. J., Jr. (1988) *Biochemistry 27*, 931–938.

Bruening, G. (1977) Plant Covirus: Two Component Systems, in *Comprehensive Virology* (Fraenkel-Conrat, H., & Wagner, H. H., Eds.) Vol. 11, pp 55–141, Plenum, New York.

Chen, M. C., & Lord, R. C. (1974) *J. Am. Chem. Soc. 96*, 4750–4752.

Chen, Z., Stauffacher, C., Li, Y., Schmidt, T., Wu, B., Kamer, G., Shanks, M., Lomonossoff, G., & Johnson, J. E. (1989) *Science 245*, 154–159.

Harada, I., Miura, T., & Takeuchi, H. (1986) *Spectrochim. Acta 42A*, 307–312.

Hartman, K. A., Clayton, N. W., Thomas, G. J., Jr. (1973) *Biochem. Biophys. Res. Commun. 50*, 942–949.

Kitagawa, T., Azuma, T., & Hamaguchi, K. (1979) *Biopolymers 18*, 451–465.

Li, Y., Thomas, G. J., Jr., Fuller, M., & King, J. (1981) *Prog. Clin. Biol. Res. 64*, 271–283.

Lord, R. C., & Thomas, G. J., Jr. (1967) *Spectrochim. Acta 23A*, 2551–2591.

Miura, T., Takeuchi, H., & Harada, I. (1988) *Biochemistry 27*, 88–94.

Nishimura, Y., & Tsuboi, M. (1986) in *Spectroscopy of Biological Systems* (Clark, R. J. H., & Hester, R. E., Eds.) Vol. 13, pp 177–232, Wiley, New York.

Nishimura, Y., Tsuboi, M., Sato, T., & Aoki, K. (1986) *J. Mol. Struct. 146*, 123–153.

Prescott, B., Sitaraman, K., Argos, P., & Thomas, G. J., Jr. (1985) *Biochemistry 24*, 1226–1231.

Sargent, D., Benevides, J. M., Yu, M.-H., King, J., & Thomas, G. J., Jr. (1988) *J. Mol. Biol. 199*, 491–502.

Semancik, J. S., & Bancroft, J. B. (1965) *Virology 27*, 476–483.

Siamwiza, M. N., Lord, R. C., Chen, M. C., Takamatsu, T., Harada, I., Matsuura, H., & Shimanouchi, T. (1975) *Biochemistry 14*, 4870–4876.

Small, E. W., & Peticolas, W. L. (1971) *Biopolymers 10*, 69–88.

Takeuchi, H., & Harada, I. (1986) *Spectrochim. Acta 42A*, 1069–1078.

Thomas, G. J., Jr. (1985) *Spectrochim. Acta 41A*, 217–221.

Thomas, G. J., Jr. (1987) in *Biological Applications of Raman Spectroscopy* (Spiro, T. G., Ed.) Vol. 1, pp 135–201, Wiley, New York.

Thomas, G. J., Jr., & Barylski, J. R. (1970) *Appl. Spectrosc. 24*, 463–464.

Thomas, G. J., Jr., & Hartman, K. A. (1973) *Biochim. Biophys. Acta 312*, 311–322.

Thomas, G. J., Jr., & Agard, D. A. (1984) *Biophys. J. 46*, 763–768.

Thomas, G. J., Jr., Medeiros, G. C., & Hartman, K. A. (1971) *Biochem. Biophys. Res. Commun. 44*, 587–592.

Thomas, G. J., Jr., Prescott, B., McDonald-Ordzie, P. E., & Hartman, K. A. (1976) *J. Mol. Biol. 102*, 103–124.

Thomas, G. J., Jr., Prescott, B., & Day, L. A. (1983) *J. Mol. Biol. 165*, 321–356.

Thomas, G. J., Jr., Prescott, B., & Benevides, J. M. (1986) *Biomol. Stereodyn. 4*, 227–254.

Verduin, B. J. M., Prescott, B., & Thomas, G. J., Jr. (1984) *Biochemistry 23*, 4301–4308.

Yu, N.-T. (1974) *J. Am. Chem. Soc. 96*, 4664–4668.